Applied Catalysis A, General 643 (2022) 118780

Contents lists available at ScienceDirect

Applied Catalysis A, General

journal homepage: www.elsevier.com/locate/apcata

Te-doped MoV-Oxide (M1 phase) for ethane ODH. The role of tellurium on morphology, thermal stability and catalytic behaviour

Agustín de Arriba [a], Benjamin Solsona [b,*], Ester García-González [c], Patricia Concepción [a], José M. López Nieto [a,*]

[a] Instituto de Tecnología Química, Universitat Politècnica de València-Consejo Superior de Investigaciones Científicas, Avenida de los Naranjos s/n, 46022 Valencia, Spain
[b] Departament d'Enginyeria Química, Universitat de València, C/ Dr. Moliner 50, 46100 Burjassot, Valencia, Spain
[c] Departamento Química Inorgánica, Facultad de Ciencias Químicas, Universidad Complutense, 28040 Madrid, Spain

ARTICLE INFO

Keywords:
Ethylene
Ethane ODH
Mo-V-O oxide
M1 phase
Tellurium

ABSTRACT

Undoped and Te-doped MoV-Oxide (M1 phase) catalysts have been prepared hydrothermally (Te/Mo ratio in the synthesis gel from 0 to 0.17; and heat-treated at 400 or 600°C in N_2 atmosphere), characterized by several physicochemical techniques and tested in the oxidative dehydrogenation (ODH) of ethane. The morphology and microporosity of the catalysts, the nature of V-species on the catalyst surface and the catalytic performance strongly depend on the composition and the heat-treatment temperature. When calcined at 400°C, the selectivity to ethylene decreases when the amount of tellurium increases, whereas when heat treated at 600°C, the selectivity to ethylene increases when the Te-loading increases. These trends have been explained on the basis of the good correlation between selectivity to ethylene and the concentration of V^{4+} species on the surface of catalysts, in which the most selective catalyst is that prepared with a Te/Mo ratio of 0.17 and heat-treated at 600°C.

1. Introduction

In the last years, the petrochemical industry has attracted a lot of attention since the decreasing use of fossil fuels and the increasing concern about global warming strikes most part of the society. Within the petrochemical industry, the production of light olefins such as propylene and, more significantly, ethylene are specially challenging because they are the main feedstock for polymer production, being polyethylene the most produced plastic polymer in the world with production rates beyond 200 million tons per year [1,2].

Nowadays, the manufacture of short chain alkenes is carried out through highly-energy consuming processes called steam cracking (pyrolysis of hydrocarbon streams) and/or fluid catalytic cracking (FCC) [2–5]. These processes (especially steam cracking), as a result of their endothermic nature, can lead to the production of up to 1.8 kg of CO_2 per kg of ethylene synthesized, which is fairly against the principles of Sustainability. On top of this, the demand of ethylene is expected to increase in the coming years, so that a lot of effort is being put on the development of new processes that could potentially replace those mentioned above in the medium term.

A different approach is the direct catalytic transformation of the corresponding alkanes in the presence of oxygen into the desired alkenes. This advantageous process, called oxidative dehydrogenation (ODH) [6–10], is exothermic, which results into lower reaction temperatures (around 400°C, compared with 700–800°C required for steam cracking) and it does not produce coke, in addition to the catalyst being regenerated in-situ by the air/oxygen stream present in the reaction environment.

At the moment, multicomponent MoVTeNbO mixed metal oxides presenting the orthorhombic crystalline phase, $(TeO)_2M_{20}O_{56}$ (M= Mo, V, Nb), the so-called M1 phase, show the best catalytic performance for the oxidative dehydrogenation of ethane (ODHE) [11–20]. For instance, the M1-MoVTeNb oxide is the catalyst that has presented the best performance in terms of selectivity (>90% in a large range of conversions) and yield to ethylene (i.e. 75% yield) [11,12]. In addition, MoV-oxide presenting the M1 phase has been also proposed as active and selective catalysts in ethane ODH, although with relatively low thermal stability [21–24]. Recent changes in catalyst preparation procedure have been also proposed, although low influence on the selectivity to ethylene has been reported [25–30].

* Corresponding authors.
E-mail addresses: benjamin.solsona@uv.es (B. Solsona), jmlopez@itq.upv.es (J.M.López Nieto).

https://doi.org/10.1016/j.apcata.2022.118780
Received 18 May 2022; Received in revised form 8 July 2022; Accepted 11 July 2022
Available online 16 July 2022

M1-containing MoV(Te,Sb)NbO catalysts were initially proposed as active and selective materials in the partial (amm)oxidation of propane to acrylonitrile and acrylic acid [31–38], which seems to be more effective in (amm)oxidation of propane than the corresponding Mo-V-O catalysts [35,39–41].

Mo-V-Te-O based catalysts present intermediate catalytic behaviour between MoVO and MoVTeNbO catalysts in propane (amm)oxidation [34,38–45]. In this case, it has been proposed that Mo and V are essential elements for the structure formation and catalytic activity, whereas the Te atoms are directly involved in the selective activation of allylic hydrogens in propylene, then optimizing its transformation to acrylonitrile or acrylic acid [37–40].

However, little is reported on the catalytic performance of Mo-V-Te-O catalysts for ethane ODH [46–48]. As a general fact, high selectivity to ethylene is achieved over samples heat-treated at 600ºC [48], but there is not available information about the effect of tellurium at low heat-treatment temperatures.

In this paper, we present, for the first time, the synthesis of Te-doped MoV-Oxide catalysts (with Te/Mo at. ratio between 0.01 and 0.17), presenting M1 phase, and their characterization, in order to establish the role of the tellurium atoms on crystal morphology, thermal stability and surface composition of catalysts as well as on the catalytic behaviour for the oxidative dehydrogenation of ethane to ethylene. The influence of both the Te-loading and the heat-treatment temperature has been studied. For comparison, it has been also studied the synthesis and catalytic performance of pure MoV-Oxide catalyst presenting M1 phase.

2. Experimental

2.1. Preparation of catalysts

Te-doped MoV-Oxides have been prepared following the hydrothermal synthesis reported elsewhere for Mo-V-Te catalyst [44]. A typical procedure consisted of mixing the metal precursors, i.e. Ammonium Heptamolybdate Hydrate (HMA, 99%, Merck), Vanadyl Sulfate Hydrate ($VOSO_4$, 97%, Sigma Aldrich) and Tellurium Dioxide (TeO_2, 99%, Aldrich) with a Mo/V/Te molar ratio of 1/0.37/x (x = 0.01–0.17). The final pH of these gels was adjusted to ca. 2. The synthesis gels were transferred to a teflon vessel coated by a stainless-steel autoclave which was kept at 175°C for 72 h. The resulting crystals were filtered off under vacuum conditions, washed with distilled water (2 ×500 mL) and dried overnight. They were washed afterwards with H_2O_2, 15 wt% for two hours (15 mL_{H2O2}:1 g_{solid}), and then filtered. The activation step was a heat-treatment under N_2 stream at 400 or 600°C for 2 h with a heating ramp of 10°C/min or 3°C/min, respectively.

For comparison, a Te-free Mo-V-O oxide was prepared hydrothermally by a procedure similar to that previously proposed [21], with a pH of the synthesis gel of ca. 3. In this case, the purification step (i.e. washed with H_2O_2 as indicated above, and filtered) took place after the thermal activation in order to improve the purity of the M1 phase. The activation step was again a heat-treatment under N_2 stream at 400°C or 600°C using the same conditions as for the Te-containing catalysts mentioned above.

The as-synthesized samples and those heat-treated at 400°C or 600°C were named as **AS-x, F-x** and **S-x**, respectively, in which "x" is the Te/Mo ratio in the synthesis gel. The characteristics of catalysts are shown in Table 1 and Table S1.

2.2. Characterization of Catalysts

N_2 adsorption isotherms were performed in a Micromeritics ASAP 2000 apparatus, where samples were degassed under vacuum conditions before adsorption. The specific surface area was determined using the BET method, whereas the micropore volume was estimated using the t-Plot method. CO_2 adsorption isotherms at 25°C were also obtained on the same apparatus in order to study the microporosity of catalysts.

Powder X-ray diffraction patterns (XRD) were collected in a PAN-analytical X'Pert PRO diffractometer with an X'Celerator dectector, using Cu-K_{alfa} radiation, in Bragg-Bretano geometry.

Crystal morphology was analysed by Scanning Electron Microscopy (SEM) in a JEOL 6300 Microscope working at a voltage of 2 kV. Average chemical composition of the samples was determined by energy-dispersive X-ray spectroscopy (XEDS) with an Oxford LINK ISIS system attached to the microscope. Each spectrum was recorded at a counting time of 120 s.

Microstructural characterization was performed by High Resolution Transmission Electron Microscopy (HRTEM) on a JEOL JEM300F electron microscope by working at 300 kV (point resolution of 0.17 nm). Crystal-by-crystal chemical microanalysis was performed by energy-dispersive X-ray spectroscopy (XEDS) in the same microscope equipped with an ISIS 300 X-ray microanalysis system (Oxford Instruments) with a detector model LINK "Pentafet" (resolution 135 eV). Samples for transmission electron microscopy (TEM) were ultrasonically dispersed in n-butanol and transferred to carbon coated copper grids.

Infrared spectra were recorded in the 400–4000 cm^{-1} region at room temperature by using a Nicolet 205xB spectrophotometer at spectral resolution of 1 cm^{-1} and 128 accumulations per scan. Previously, all the samples were milled and mixed with KBr (spectroscopic grade) and pressed into pellets.

Raman spectra were performed with an inVia Renishaw spectrometer with an Olympus microscope hitched, and the wavelength was set to 514.5 nm (generated with a Renishaw HPNIR laser with a power of 15 mW on the sample).

Temperature-programmed reduction ($TPR-H_2$) experiments were carried out in a Micromeritics Autochem 2910 gadget, equipped with a TCD detector. The reducing gas composition consisted of 10% H_2 diluted

Table 1
Characteristics of Te-doped MoV-Oxides catalysts.

Catalyst	Te/Mo ratio	N_2-adsorption		CO_2-adsorption	H_2-TPR	TPD-NH_3
	in the synthesis gel	Surface area (m^2g^{-1})[a]	T-plot Micropore volume ($10^3 \cdot cm^3/g$)[a]	Surface area ($m^2\ g^{-1}$)	TMR (°C)[b]	NH_3 desorption ($\mu mol_{NH3}/g_{cat}$)[c]
F-0	0.00	35.2	10.9	68.9	465	551.8
F-0.01	0.01	60.0	16.9	n.d.	450	nd
F-0.05	0.05	44.4	15.4	73.7	412	649.1
F-0.10	0.10	45.0	4.7	62.0	408	640.2
F-0.17	0.17	20.3	2.5	45.8	400	167.0
S-0	0.00	7.2	1.7	n.d.	n.d.	123.2
S-0.01	0.01	17.9	2.8	n.d.	470	n.d.
S-0.05	0.05	12.9	3.5	35.6	479	186.4
S-0.10	0.10	13.5	3.0	27.8	517	121.8
S-0.17	0.17	7.9	1.9	28.3	502	160.8

[a] Surface area and Micropore volume were calculated by BET and t-Plot methods, respectively, after N_2 adsorption isotherm;
[b] TMC= Temperature, in °C, of the maximum hydrogen consumption during TPR experiment.
[c] Amount of ammonia chemisorbed at 100°C during the NH_3-TPD experiment, per gram of catalyst (measured in standard temperature and pressure).

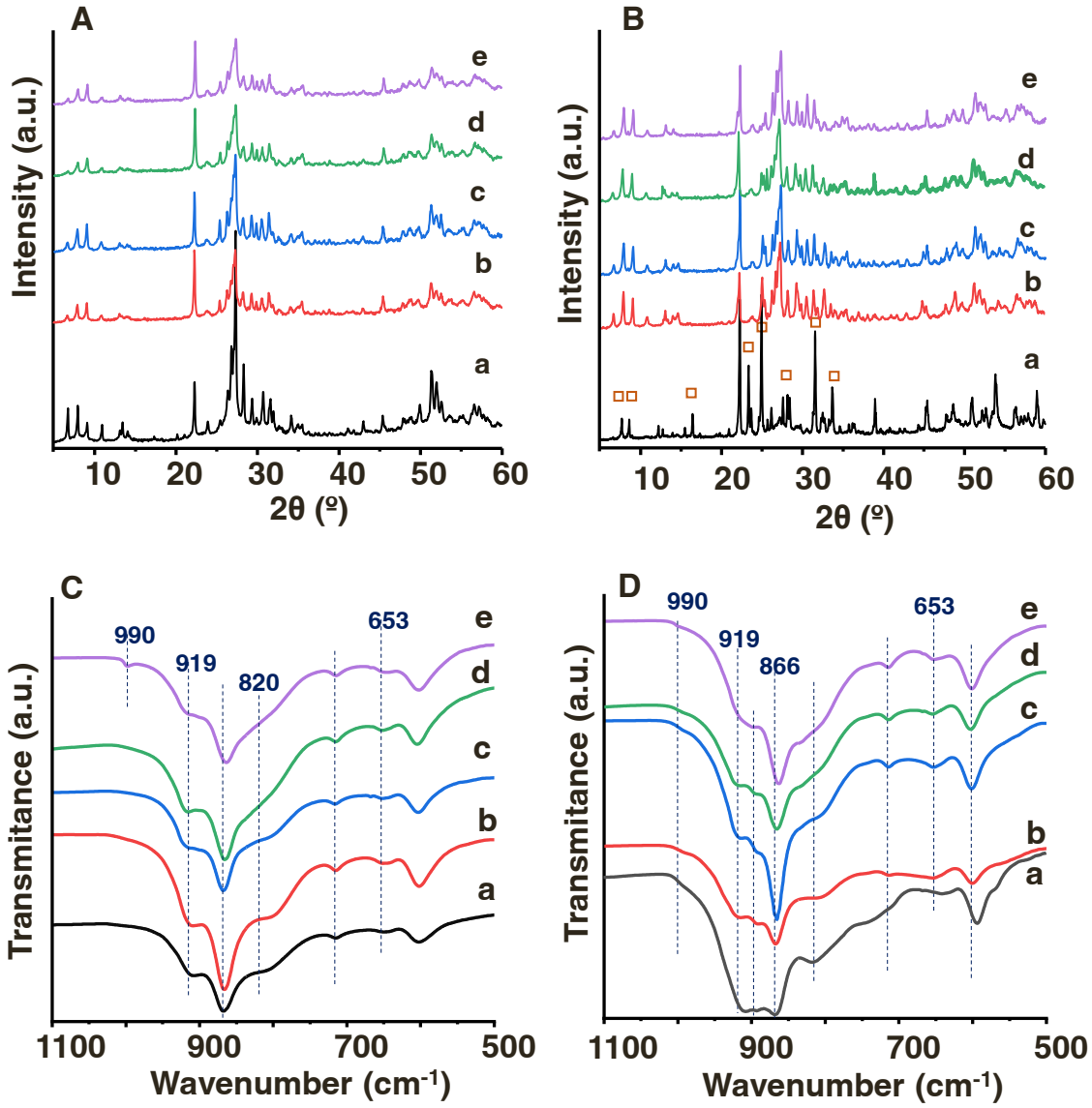

Fig. 1. XRD patterns (A, B) and FTIR spectra (C, D) of catalysts, heat-treated at 400°C (A, C) or at 600°C (B, D). Samples prepared with Te/Mo ratio in the synthesis gel of: 0.0 (a); 0.01 (b); 0.05 (c); 0.10; (d) or 0.17. Symbols: $(Mo_{0.93}V_{0.07})_5O_{14}$□ (□).

in Ar, with a total flow rate of 50 mL/min. Samples were heated until 600°C, at a 10°C/min heating rate.

XPS analysis were carried out on a SPECS spectrometer equipped with a Phoibos 150 MCD-9 detector using a monochromatic X-ray source (Al K_{alfa}- 1486.6 eV) and recording spectra via analyser pass energy of 50 eV, an X-ray power of 100 W, and operation pressure of 10^{-9} mbar. Data was treated by using CASA XPS software, with binding energies referenced to C *1s* at 284.5 eV.

Temperature programmed desorption of ammonia (TPD-NH_3) experiments were performed in a Micromeritics TPD/2900 equipment. About 50 mg of sample was heated at 300°C, under argon flow, for 1 h. Cooled down to 100°C and afterwards saturated with ammonia. Then, samples were kept under inert gas flow at 100°C for 15 min in order to desorb the physically adsorbed NH_3. The TPD analysis was carried out in the 100–500°C temperature range, using a heating rate of 10°C, while desorbed NH_3 was analysed by both a mass spectrometer and a thermal conductivity detector analyser.

2.3. Catalytic tests

Catalytic tests for the ODHE were conducted in a tubular isothermal flow reactor, with temperatures ranging from 300 to 400°C. A reaction mixture of C_2H_6/O_2/He with molar ratio of 5/5/90 was fed to the reactor, varying contact times by modifying the total flow and/or the loading of catalyst (25–100 mL min^{-1} and 0.05–1.00 g, respectively). The catalytic bed kept a constant volume by adding different amounts of silicon carbide mixed with the catalyst. Reaction products were followed by gas chromatography, with the chromatograph consisting of two packed columns [48]: i) a molecular sieve 5 Å (2.5 m) and ii) a Porapak Q (3 m). Blank tests showed no catalytic activity for the temperature range studied.

3. Results and discussion

3.1. Physicochemical characterization of catalysts

The main characteristics of the catalysts, samples heat-treated at 400ºC or 600ºC in N_2 atmosphere, are presented in Table 1.

XRD patterns of as-synthesized samples (**AS**-series) show the presence of all characteristic diffraction peaks of the orthorhombic M1 phase (i.e., peaks at 2θ= 6.7°, 7.9°, 9.0°, 10.8°, 23.0° and 27.3°) (Fig. S1, supporting information). This demonstrates that M1 phase is the main

constituent of catalysts in the presence/absence of tellurium, in agreement to previous results [20–24,42–48]. On the other hand, the thermogravimetric analyses of as-synthesized samples are shown in Fig. S2. In general, these samples present weight losses, in the region between 50 and 200°C and between 250 and 400°C, which are related to the loss of H_2O and H_2O/NH_3, respectively. In addition, it is observed that the weight loss in the temperature range of 250–400°C decreases with the increase of Tellurium in the catalyst.

The XRD patterns of catalysts heat-treated at 400°C (**F**-series) and 600°C (**S**-series) are presented in Fig. 1. All catalysts heat-treated at 400°C presented M1 phase as majority, although the presence of other crystalline phases as minority can be observed depending on the Te-content and/or the activation temperature.

Thus, in the case of **F-0**, the M1 phase is the main crystalline phase, with no appreciable formation of other crystalline phases. The catalysts with different Te-contents maintain the structure of the M1 phase in samples heat-treated at 400°C (Fig. 1 A), probably due to the high stability of the Te-O chains in the hexagonal channels [35,38,41,50].

On the other hand, several changes have been observed for catalysts heat-treated at 600°C (Fig. 1B). Then, in the case of the Te-free sample (**S-0**) the main crystalline phase discriminated is $(Mo_{0.93}V_{0.07})_5O_{14}$, with diffraction peaks at 2θ= 22.3, 25.0, 31.6 and 33.7° [26,33,49–51]. Diffraction peaks of the M1 phase can be also detected although with very low intensity. Conversely, the M1 phase is almost the only crystalline phase observed in all the Te-containing catalysts, with the minor presence of $(Mo_{0.93}V_{0.07})_5O_{14}$ or $(V_{0.95}Mo_{0.97})O_5$. Accordingly, this indicates that the presence of Te^{4+} atoms strongly improves the thermal stability of the M1 phase (up to 600°C), even in samples with very low Te/Mo ratios [49,51].

Fig. 1 C and 1D show the IR spectra of **F-** and **S**-series, respectively, in the low frequency region (1100–500 cm^{-1}). Bands at 603, 653, 714, 866 and 919 cm^{-1} for both series indicate the presence of the M1 phase, as previosly reported [33,44,52]. Specifically, the signal at 919 cm^{-1} corresponds to (Mo,V)-O (terminal oxygen) bond, whilst signals at 603, 653, 714 and 866 cm^{-1} correspond to antisymmetric Mo-O-X vibrations, where X=Mo, Te. In the case of the **S**-series, a new signal at wavenumber 896 cm^{-1} appears in **S-0.01**, **S-0.05** and **S-0.10**, being very weak for **S-0.17**, which corresponds to the minor presence of the $TeMo_5O_{16}$ phase [33], in addition to further signals at 820 cm^{-1} and 990 cm^{-1}, which correspond to MoO_3 [33], appearing the latter also in the sample with the highest tellurium content treated at 400°C (**F-0.17**).

Raman spectra of both series confirm the above results (Fig. S3). Accordingly, for all catalysts, it can be observed a main band at ca. 869 cm^{-1}, related to the M1 phase [53–55], although well defined signals at 993 and 819 cm^{-1} (attributed to the minor presence of MoO_3 in the catalyst [56,57]) are also observed for sample **F-0.17**. In the case of the catalysts of the **S**-series with low and medium Te-loading (i.e. samples **S-0.01** to **S-0.10)**, an additional weak peak at ca. 987 cm^{-1} is observed, which is associated with the minor presence of the pseudo-hexagonal $TeMo_5O_{16}$ phase [33].

Samples were further investigated by high resolution transmission electron microscopy (HRTEM) and the results were compared with those observed in the FESEM images. Fig. 2 (A to E) shows the two types of micrographs for samples of **F**-series. The similarity in crystal morphology can be observed through the series and the characteristic rod like morphology is easily recognized for any composition in the FESEM images. However, HRTEM images show significant differences. The low magnification image on Fig. 2 F corresponds to **F-0** catalyst; it can be observed that rods are actually formed by nanocrystallites that start assembling to become single crystal rods. When introducing tellurium, even from the lowest concentration, particles are in fact bunches of coalescent rod-like crystallites which progressively grow for increasing tellurium amounts. Right-side images on Fig. 2 (HRTEM micrographs A to E) illustrate this observation and the coalescence of bigger crystals gives rise finally to single crystal rods in **F-0.17** catalyst. Thus, the incorporation of Te in the structural framework modifies the crystal growth mode and crystallinity. HRTEM images on **S**-series, do not show significant differences associated to Te content, crystals differing only in size but always maintaining the same morphology. Fig. S8 shows selected FESEM micrographs corresponding to characteristic samples of the **S**-series**.** Features observed in the crystals growth habit are in agreement with all the above although in the case of **S-0**, different crystal morphologies associated with the thermal decomposition of M1 were observed.

The specific surface area of Te-doped MoV-Oxides catalysts was studied by N_2- and CO_2-adsorption isotherms (See Table 1 and Table S1, and Figs. S4 to S7). In order to estimate both the BET surface area and the micropore volume values, the t-Plot method was applied to the N_2 adsorption isotherms [20,23,30,58,59]. Results for **F**-series and **S**-series of catalysts are presented in Table 1 **(**and Figs. S4A and S4B), while the

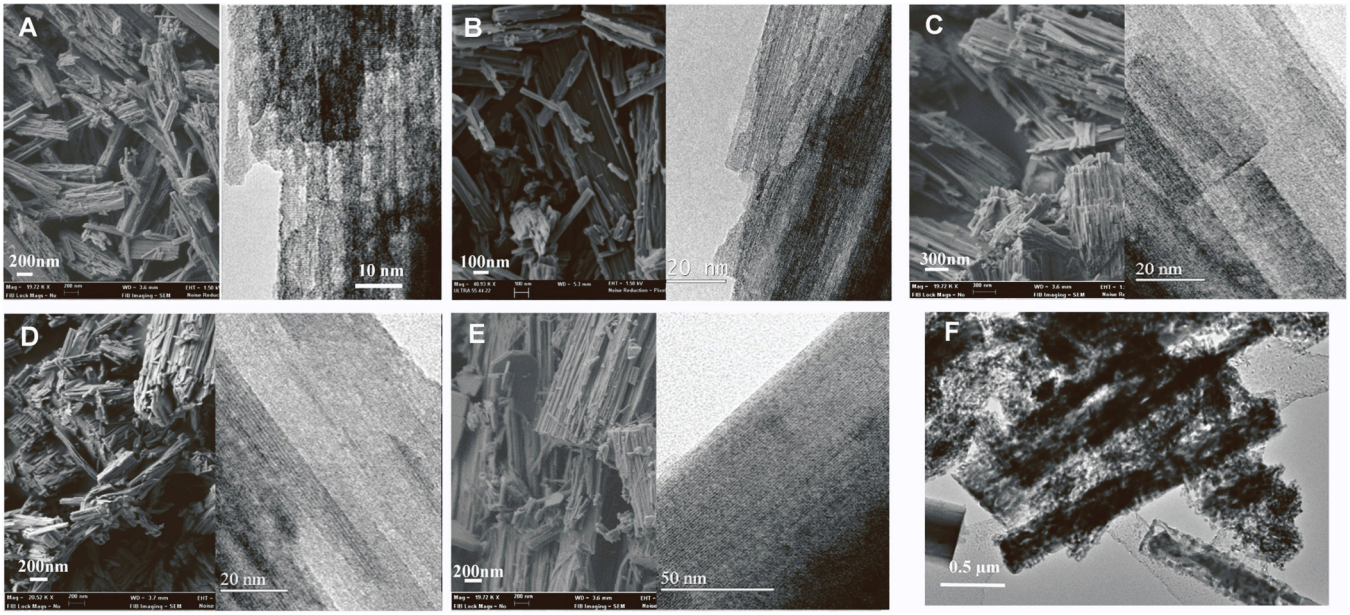

Fig. 2. (A-E) FE-SEM (left) /HRTEM (right) micrographs of catalysts **F-0**, **F-0.01**, **F-0.05**, **F-0.10** and **F-0.17**, respectively. **(F)** Low magnification TEM image showing a group of crystals of **F-0**.

Table 2
XPS of Te-free and Te-containing Mo-V-O catalysts.

Catalyst	Mo/V/Te atomic ratio		XPS results			
	EDX	XPS	Mo^{6+}/ Mo_{total} (%)	Te^{4+}/ Te_{total} (%)	V^{4+}/ V_{total} (%)	Me/O ratio
F-0	0.73/ 0.27/ 0.00	0.86/ 0.14/ 0.00	100	0	73.4	22.0/ 78.0
F-0.01	0.73/ 0.26/ 0.02	0.86/ 0.13/ 0.02	100	100	64.3	27.3/ 72.8
F-0.05	0.70/ 0.26/ 0.04	0.80/ 0.16/ 0.03	100	100	59.0	31.6/ 68.4
F-0.10	0.70/ 0.25/ 0.05	0.80/ 0.15/ 0.05	100	100	52.7	32.3/ 67.7
F-0.17	0.73/ 0.19/ 0.08	0.85/ 0.07/ 0.08	100	100	43.7	32.5/ 67.5
S-0	n.d.	0.89/ 0.11/ 0.00	100	0	34.4	31.2/ 68.8
S-0.01	0.71/ 0.28/ 0.01	0.85/ 0.14/ 0.01	100	100	20.3	28.7/ 71.3
S-0.05	0.70/ 0.27/ 0.03	0.82/ 0.15/ 0.03	100	70.4	19.5	31.0/ 69.0
S-0.10	0.71/ 0.25/ 0.05	0.81/ 0.14/ 0.05	66.2	65.8	61.9	31.9/ 68.1
S-0.17	0.73/ 0.21/ 0.06	0.82/ 0.14/ 0.04	100	100	62.6	31.9/ 68.1

corresponding t-Plot calculations are presented in Figs. S5A and S5B.

Differences in surface area along the series are significant, the maximum being obtained for **F-0.01** and then a slight decrease for **F-0.05** and **F-0.10** samples, the value for **F-0.17** being the lowest (see Table 1 and Fig. S6). The observed variations are in accordance with the microstructural characteristics of catalysts and follow a similar sequence than that of the micropore volume. Thus, access to micropores seems to be optimal in **F-0.01**. However, although small tellurium amounts may be sufficient to favour M1 crystallization, it is not large enough to cause appreciable blockage of the hexagonal and heptagonal cavities, resulting in the highest volume of micropore of the series.

Noteworthy, for samples heat-treated at 400°C, BET surface areas increase initially when tellurium content increase, showing a maximum for the sample **F-0.05**. Indeed, very little tellurium promotion of the M1 phase (i.e. **F-0.01** and **F-0.05**) leads to surface areas ca. 1.5–2 times bigger compared to that obtained for **F-0** (35.2 and 60.0 $m^2\ g^{-1}$ for samples **F-0** and **F-0.01**, respectively). However, higher Te-contens cause a decrease of the surface area. For instance, the surface area of **F-0.17** is ca. 1.7 times lower than that of **F-0** (Table 1). Therefore, it is suggested that high tellurium contents will block hexagonal channels but also partially the heptagonal channels of the M1 structure [49], resulting in a decrease in the surface area. In any case, the hydrothermal synthesis of this type of oxides can lead to materials with low or high surface area depending on the composition of the material and the thermal activation procedure [21–24,44,59].

Interestingly, significant differences are also observed in the micropore volume, where these values initially increase with the tellurium content up to **F-0.05**, and then, the micropore volume values drastically decrease (Table 1**)**. In fact, although maintaining a considerably large surface area, the micropore volume for the sample **F-0.10** decreases drastically, suggesting that, from this composition, a greater proportion of the heptagonal cavities are blocked and/or may be due to changes in the morphology of particles.

On the other hand, and as a consequence of the thermal activation, larger differences are observed for **F-0**, where a pure M1 phase leads to a BET surface area of 35.2 m^2/g, in contrast to **S-0,** with very low surface area (7.2 m^2/g). Although comparable values were obtained for **F-0.17** and **S-0.17** samples (Table 1), both surface area and micropore volume values for the **S**-series are much lower compared to those obtained for the **F**-series, where the biggest differences were found for the Te/Mo ratios of 0.01 and 0.05. Thus, the micropore volume values are ca. 6 times higher for the **F**-series than for the **S**-series.

The above results show that this low activation temperature (400°C) leads to materials with higher micropore volume [21–23,59,61], especially the ones with lower tellurium content.

In order to get further insights into the microporous characteristics of the M1 phase oxides, CO_2 adsorption isotherms were recorded for the most representative catalysts. Although the use of CO_2 also has some drawbacks, the use of CO_2 isotherms is an interesting alternative for materials with very small pores in which the molecules of N_2 cannot access at cryogenic temperatures [60–63]. Experimental isotherms are plotted in Fig. S5, and values of surface area and micropore volumes are presented in Table 1. In this sense, by using CO_2 as a probe molecule instead of N_2, a more appropriate set of values for both the surface areas and the micropore volume of materials with small micropores can be obtained [22,58]. In addition to this, a non-microporous material such as molybdenum trioxide (i.e. α-MoO_3) was used as a reference to ascertain the speculated microporosity of the materials.

The highest adsorption occurs by adding small amounts of tellurium into the catalyst (**F-0.05**), and this adsorption slightly decreases when increasing tellurium content (**F-0.10**), to a point that the sample adsorbs less than the catalyst without tellurium in the structure, as in the case of **F-0.17 (**Fig. S7-A**)**. Nevertheless, if the tellurium content keeps rising, all the hexagonal channels would be filled with -O-Te-O- chains, resulting in the less microporous nature of **F-0.17**. However, very low microporosity is observed in samples heat-treated at 600ºC (Fig. S7-B), in agreement with previous results [44].

In addition to this, it must be noted that surface areas values for the CO_2 adsorption isotherms are significantly higher than those obtained with the N_2 adsorption isotherms, in all cases, being almost the double and even more. For instance, a value of 68.9 $m^2\ g^{-1}$ is obtained from CO_2-adsorption for **F-0**, whereas 35.2 $m^2\ g^{-1}$ is the value obtained from N_2-adsorption. These results highlight the marked microporosity nature of the samples that present the M1 crystalline phase. This is in agreement with previous results reported on MoV oxides [21–24,59] and MoVTeNb-mixed oxides [59] containing M1 phase which show one-dimensional micropores of size similar to C_2H_6 but much smaller than C_6H_{12} [22,59], and in which the catalyst preparation methods significantly affect their elemental composition but also the accessible micropore volumes and surface areas [21–24,59].

The near surface region of catalysts of both the **F-** and the **S**-series were also studied by XPS and analytical results are comparatively presented in Table 2. Fig. 3 shows the XPS spectra of the V $2p_{3/2}$ core level for the **F**-series (Fig. 3A) and the **S**-serie**s** (Fig. 3B) catalysts. All catalysts presented two classical signals related to the simultaneous presence of V^{4+} (B.E. of 515.9 eV) and V^{5+} (B.E. of 517.0 eV) species [28,33,36,39,64–68]. However, clear differences can be discriminated in both set of catalysts depending on the composition and the thermal activation of the sample.

On one hand, by looking at the samples heat-treated at 400°C, the relative intensity of the V^{5+} signal increases with the tellurium content, thus being the predominant in the **F-0.17** sample, whereas V^{4+} species seems to be the major species in **F-0**. Therefore, lower tellurium contents seem to favor an enrichment in V^{4+} species.

On the other hand, V $2p_{3/2}$ core level results for the catalysts heat-treated at 600°C show the opposite trend (Fig. 3B). In this case, V^{5+} species were majority in the samples with the lowest tellurium contents. Increasing tellurium amounts led to a higher concentration of V^{4+},

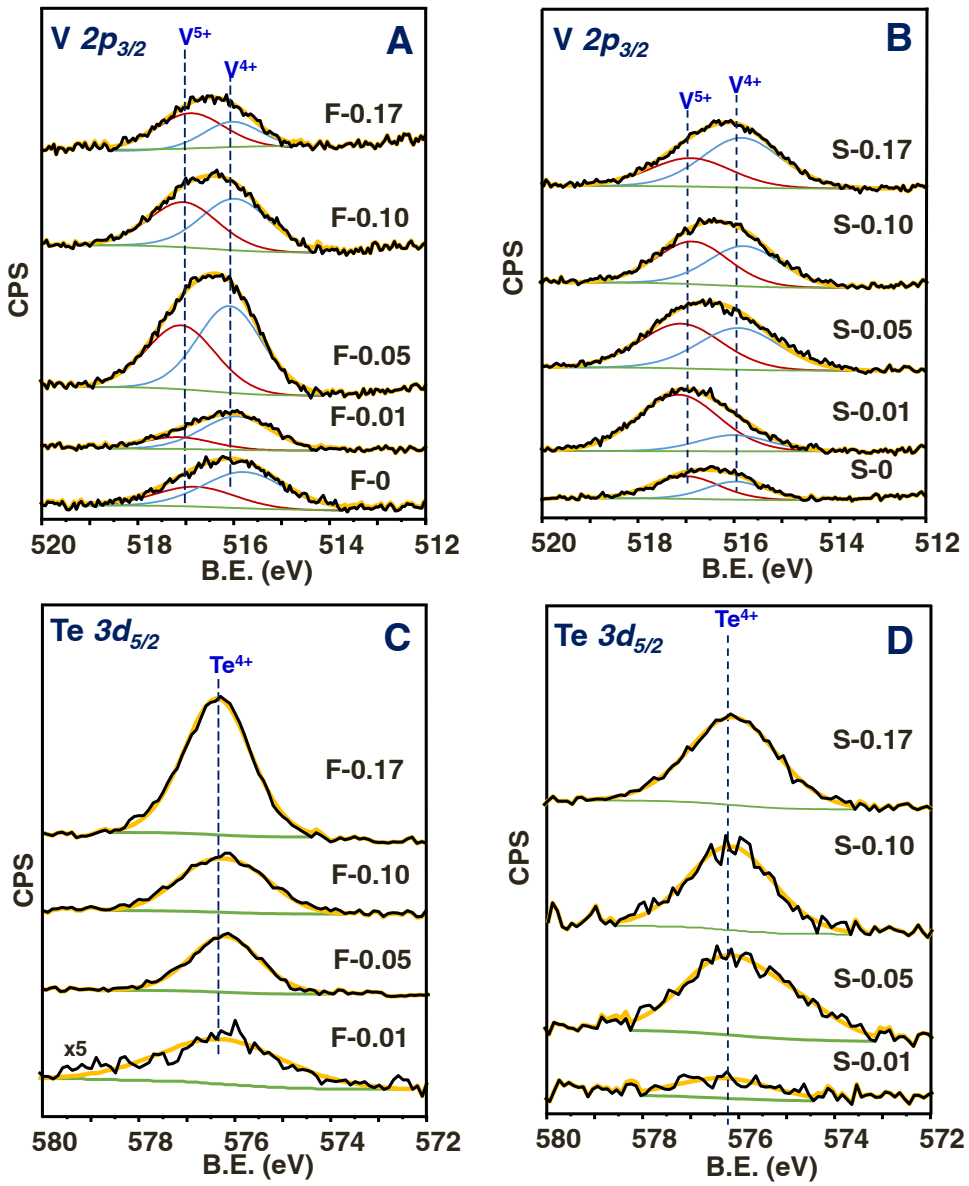

Fig. 3. V $2p_{3/2}$ (A, B) and Te $3d_{5/2}$ (C, D) XPS spectra of catalysts heat-treated at 400°C (A, C) or 600°C (B, D).

obtaining its highest relative intensity in the sample **S-0.17**. Therefore, in this set of catalysts, it is suggested that the presence of tellurium may avoid the segregation of V^{5+} species in the hexagonal channels, especially at higher activation temperatures, as proposed for MoV-O catalysts [24,66].

Fig. 3 C and 3D show the XPS spectra of the Te $3d_{5/2}$ core level analyses of the **F**- and **S**-series, respectively. For the catalysts heat-treated at 400°C, a single symmetrical signal centered at 576.3 eV is observed, suggesting the unique presence of Te^{4+} species into the structure [27, 33]. Likewise, an unique signal can be deconvoluted for the catalysts of the **S**-series, as can be seen in Fig. 3D.

Mo *3d* core level spectra for catalysts heat-treated at 400 or 600°C are shown in Figs. 4A and 4B, respectively. For the **F**-series (Fig. 4A), a single signal with two components at ca. 232.5 eV, assigned to the Mo $3d_{5/2}$ core level, and a second component corresponding to Mo $3d_{3/2}$ core level, with spin orbit component separated by 3.15 eV, is seen for all the catalysts, corresponding to Mo^{6+} species as reported elsewhere [27,28,33,66–69]. Similarly, Mo *3d* signals for the **S**-series showed only one signal related to the presence of Mo^{6+} (Fig. 4B).

Fig. 5 shows the variation of the Te/Mo and V/Mo ratio with the Te/Mo proportion in the synthesis gel as determined by EDX (Fig. 5A) and XPS (Fig. 5B) for the **F**-series. In all cases, the Te/Mo ratio increases when increasing the Te-content in the synthesis gel. However, the V/Mo ratio presents a maximum for samples with Te/Mo ratio in the synthesis gel of ca. 0.05, decreasing for higher Te/Mo synthesis ratios. Accordingly, the presence of Te^{4+} cations in the catalyst, which are mainly incorporated from the synthesis in the hexagonal channels forming –Te-O-Te infinite chains [32], disfavours the incorporation of V in the hexagonal positions, as suggested for Te-free MoVO (M1) catalysts [24,67]. Furthermore, similar relationships for the catalysts of the **S**-series are presented in Fig. 5C (EDX) and Fig. 5D (XPS). In those figures, it can be seen the same trend observed for the **F**-series, although less marked, due to the loss of tellurium associated to the severe thermal treatment for these catalysts. Nevertheless, it must be noted that, unlike the reference catalyst calcined at 400°C (i.e. **F-0.17**), the amount of V species determined by XPS in the **S-0.17** catalyst does not drastically decrease, suggesting that, in this catalyst (controlling both the composition and, more importantly, the activation temperature) there is not a blockage of the vanadium cations by the incorporation of tellurium into the structure.

On the other hand, and according to HRTEM results (Fig. 2) and

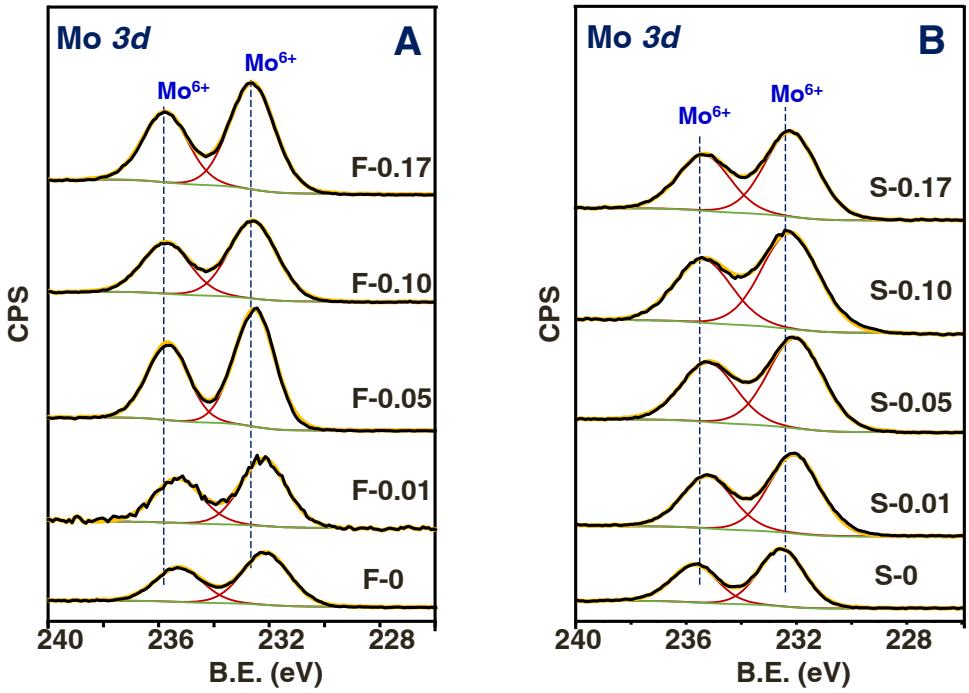

Fig. 4. Mo 3d (A, B) XPS spectra of catalysts heat-treated at 400°C (A) or 600°C (B).

adsorption of N_2 and CO_2 (Figs. S5 and S7, supplementary information), the incorporation of small amounts of tellurium favours changes in the crystal growth and microporosity. In this sense, surface area initially increases when a small amount of tellurium is added (i.e. Te/Mo in gel of 0.01) and then it declines when increasing the Te-content. Moreover, those catalysts prepared with Te/Mo ratio in the synthesis gel between 0 and 0.05 show the highest proportion of micropore area, especially that with Te/Mo ratio of 0.05, in which 73% of its area corresponds to micropore.

Therefore, the presence of a relatively low amount of Te^{4+} atoms in the hexagonal channels seems to be very important to increase the thermal stability of the orthorhombic M1 phase catalysts. Then, as observed in Fig. 1B, in the Te-containing catalysts the M1 phase remain as the main crystalline phase for samples heat-treated at 600°C. However, for the corresponding Te-free catalyst, sample **S-0**, the M1 phase is transformed into other mixed metal oxides, $(Mo,V)_5O_{14}$-type during the heat-treatment at 600°C (Fig. 1B, pattern a).

Fig. 6 shows the H_2-TPR profiles of the catalysts of **F**-series (Fig. 6A) and **S**-series (Fig. 6B**).** For the **F**-series, the temperature for the first reduction peak decreases when increasing the tellurium content in the catalyst (Table 1 and Fig. 6A), thus appearing from 470°C (for **F-0**) to 420°C (for **F-0.17**). However, for catalysts in the **S**-series, the differences in the temperature of the first reduction peak are negligible (Fig. 6B).

It must be noted that, for the **F**-series, the onset of the reduction temperature decreases when increasing the Te-content. An opposite trend for the onset and maximum temperature is observed in the case of the **S**-series, where the temperature at which the reduction starts follows the trend: **S-0.01** < **S-0.05** < **S-0.10** < **S-0.17**. In addition to this, the reducibility of the samples treated at 400°C (**F**-series) seems to be higher than those observed in catalysts of the **S**-series, since a clear reduction profile of **F**-series catalysts starts to be seen at temperatures around 300°C, in contrast with catalysts of the **S**-series, in which that reduction barely starts around 400°C.

Furthermore, acidic characteristics of catalysts have been studied by NH_3-TPD. It is well known that acid properties of M1-based catalysts strongly depend on the catalyst composition [67,68]. The NH_3-TPD profiles for **F-** and **S**-series are displayed in Figs. 6C and 6D, respectively, wheras the ammounts of NH_3 adsorption on these catalysts are presented in Table 1. It must be noted that these results have been normalized by BET surface area (Fig. 6, C and D), whereas those normalized per weigth of catalyst are shown in Fig. S10 (supplementary information).

For catalysts heat-treated at 400°C, the highest number of acid sites (which corresponds with the greater amount of NH_3 desorbed, see Table 1) is reached for the catalyst without Te (**F-0)** when normalized per surface area (Fig. 6C) and for **F-0.05**, if normalized per mass of catalyst (Fig. S10). Additionally, a shift towards lower temperature of the maximun of ammonia desorption is observed for samples with high Te-content, which means that the amount of tellurium also influences the strength of the acid sites. Therefore, both the number of acid sites and their strenght decrease when increasing tellurium content.

The amount of NH_3 desorbed follows a similar trend in the **S**-series (Fig. 4D), if we take the values normalized by BET surface area, although they are fairly lower than those of the **F**-series (Fig. 4C). Especially notorius is the case of the sample **S-0.17**, which is not only the one presenting the highest amount of ammonia desorbed of the series, but also the ammonia desorbed is more than two times that of its **F**-counterpart. In addition to this, it must be noted that the Te-free catalyst (**S-0**), presents a higher amount of ammonia desorbed than **F-0**, despite the decomposition of the M1 phase, althought the plot may look different as a result of the normalization. Moreover, if a comparison is stablished between the strenght of the acid sites in the samples treated at 400 and 600°C, it can be seen that the maximum shifts to lower temperatures in the **S**-series counterpart (i.e. acid sites with lower acid strenght).

From all the above, it seems clear that the Te content has a strong influence on crystal growth but also on the surface area and microporosity, these effects being more important in the case of samples heat-treated at 400°C. In addition, an influence of the presence of Te on the amount of surface V^{4+} species is also observed for catalysts heat-treated at 600°C (Table 2). A similar influence of the heat-treatment conditions on the concentration of surface V^{4+} species has been also observed in the case of MoVTeNbO catayst [44]. In this sense, it is reported that V^{4+} species tend to locate around hexagonal and heptagonal channels [49] which is where tellurium atoms are placed, thus hindering the access to the microporosity. Therefore, the greater the amount of tellurium present for samples heat-treated at 400°C, the lower is the

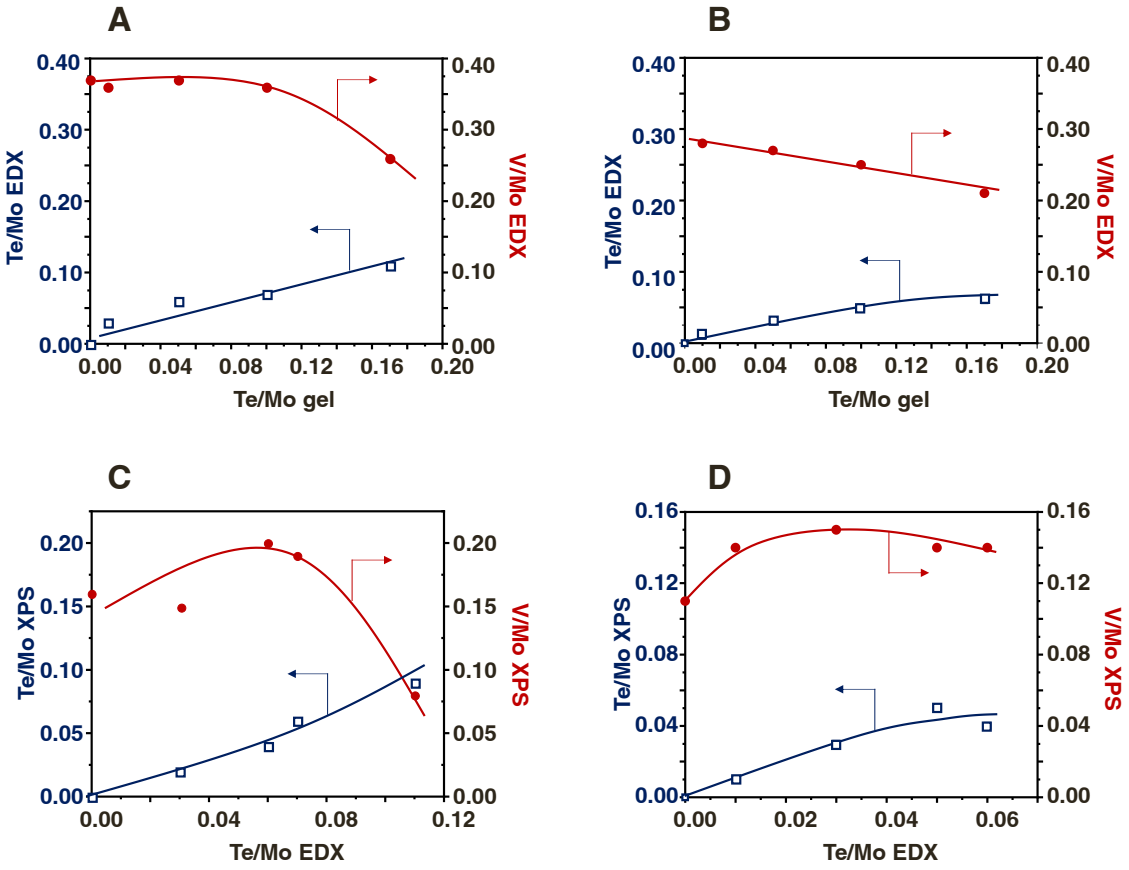

Fig. 5. Variation of the Te/Mo (□) and V/Mo ● (●) atomic ratio (determined by EDX) with the Te/Mo ratio in the synthesis gel in catalysts heat-treated at 400°C (A) or 600°C (B). Variation of the Te/Mo (□) and V/Mo ● (●) atomic ratio (determined by XPS) with the Te/Mo atomic ratio determined by EDX in catalysts heat-treated at 400°C (C) or 600°C (D). Characteristics of catalysts in Table 1.

accesibility of the V^{4+} species, this way weakening the acid properties of the catalyst.

3.2. *Catalytic results of $MoVTe_x$ samples*

Te-free and Te-containing Mo-V-O catalysts have been studied in the ethane ODH, in the 350–400°C reaction temperature range. The catalytic results at a contact time, W/F, of 16.0 (**F**-series) or 65.0 g_{cat} h $(mol_{C2H6})^{-1}$ (**S**-series) are comparatively shown in Table 3. It can be seen that the catalytic activity per gram of catalyst is remarkably higher in the case of the catalysts heat treated at low temperature.

Fig. 7 shows the variation of the specific activity (activity normalized per surface area) with the Te/Mo atomic ratio in the synthesis gel for catalysts heat-treated at 400°C (Fig. 7A) or 600°C (Fig. 7B). The higher activity of the **F**-series is related to the larger surface area, but other factors must be present since, on average, the specific activity is still around one order of magnitude higher than in the **S**-series (except for samples with high Te-loading). Unexpectedly, in the catalysts with the highest Te-loading the specific activity is higher if the heat-treatment temperature is 600°C. Considering both series separately, the catalytic trends are different. Thus, in the **F**-series, the specific activity firstly increases with the tellurium content until Te/Mo= 0.05 at. ratio, and then it decreases for **F-0.10** and **F-0.17**. However, for the **S**-series, a continuous increase of the specific activity is observed when the Te-loading increases. Fig. S11 also presents the evolution of the STY_{C2H4} (formation rate of ethylene), showing a similar trend to that observed with the specific activity.

Fig. 8 shows the variation of the selectivity to ethylene with the ethane conversion in isothermal conditions for samples heat-treated at 400°C or 600°C. It can be seen that the selectivity to ethylene presents different values depending on the nature of the catalyst. The main difference lies on the initial selectivity (at low alkane conversions) since, for all cases, drops with similar slopes are observed when increasing the ethane conversion.

We have also studied the stability of two representative catalysts (**F-0** and **S-0.17**) with the reaction conditions of Table 3. For both catalysts a highly stable performance, without apparent decrease of neither the catalytic activity nor selectivity to ethylene, was observed after 8 h on line.

3.2.1. *Relationship between physicochemical properties of the catalysts and the catalytic results*

As shown above, both the Te-loading and the activation temperature exert a determining role in the catalytic performance of MoVTeO catalysts. However, both factors have to be considered together since, otherwise, the trends observed are dissimilar.

Fig. 9A shows the variation of the selectivity to ethylene (at a fixed reaction temperature and ethane conversion of ca. 40%) with the Te/Mo at. ratio in the synthesis gel. Surprisingly, the effect of the amount of tellurium in the catalyst over the selectivity to ethylene highly depends on the heat-treatment temperature of catalysts (Fig. 8). In fact, both catalysts series present an opposite trend. Then, for the catalysts heat-treated at 400°C (**F**-series), lower contents of tellurium favor a higher selectivity to ethylene, being the catalysts with he highest content (i.e. **F-0.10** and **F-0.17**) the ones that present the lowest selectivity to ethylene. Nevertheless, for the **S**-series, the selectivity to ethylene increases as the tellurium content increases: **S-0.17** > **S-0.10** > **S-0.05** > **S-0.01** > **S-0**. A similar trend to that observed for samples **F-0.17** and **S-0.17** has been also reported for propane oxidation over MoVTeO catalysts, in which the higher the calcination temperature the higher the selectivity to acrylic

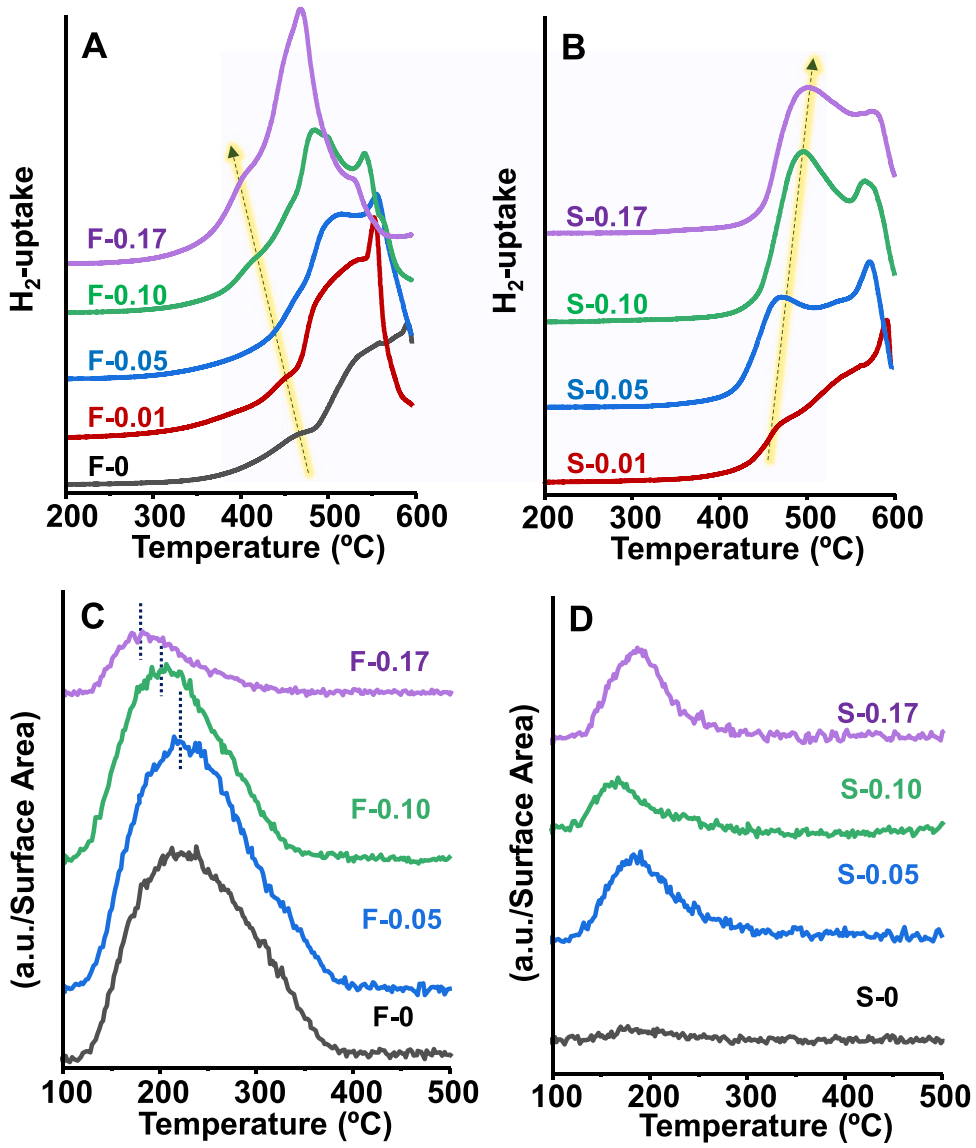

Fig. 6. H_2-TPR (A, B) and NH_3-TPD (C, D) patterns for the catalysts heat-treated at 400°C (A, C) or 600°C (B, D).

acid was [44].

According to our results, it can be concluded that the incorporation of Te^{4+} in the framework of M1-phase changes the crystal growth mode and crystallinity, thus modifying the surface area and the microporosity. As a consequence, it has a determining influence on the catalytic properties.

In the present article, it has been observed that the most selective catalysts heat treated at 400°C are those that present the highest proportion of micropore area. This observation is in agreement with that suggested by Annamalai et al. [59], which observed that in the micropores of the M1 phase the ethane molecule is more selectively activated that in the external surface. This positive catalytic feature of the micropores of the M1 phase was ascribed to the Van der Waals stabilization of tightly confined ethane and ethylene molecules, preventing the O-insertion, with the consequent carbon oxides formation. This difficult O-insertion was related to the curvature of the micropores and the steric hindrance at bridging O-atoms [59,66]. However, this trend is not clearly observed for the samples heat treated at 600°C, although the catalyst with the highest proportion of micropore area is the one that reaches the highest selectivity to ethylene.

The oxidation state of V species on the catalyst surface has been reported to be related to the catalytic performance, especially to the selectivity to ethylene [69,70]. Therefore, differences in the selectivity to ethylene during the ethane ODH are expected when comparing the catalysts of both series. In this sense, it has been proposed that, in Mo-V-O (M1 phase), V atoms can be present in hexagonal channels when the samples are heat-treated in an inert atmosphere, N_2 or Ar [24,69], whereas V is not present in the hexagonal channels when samples are calcined in oxygen [22,24]. Vanadium migration into the hexagonal channels seems to occur during the heat-treatment in the absence of oxygen [24], or in the presence of steam [69].

On the other hand, by taking into account the changing microstructure and microporosity that occurs along the series, these results may demonstrate that, in addition to chemical composition, micropore volume plays a relevant role in the selectivity to ethylene of the catalyst, probably related to the presence of certain active species in the proximity of hexagonal/heptagonal cavities responsible for microporosity. In this sense, it is reported that V^{4+} tends to locate around those cavities [38] and, in these series, the amount of V^{4+} varies inversely with the tellurium content (for catalysts heat-treated at 400°C), which is precisely located in these cavities. Accordingly, for catalysts activated at 400°C, the concentration of V^{4+} reaches a maximum when there is no tellurium in the catalyst (sample **F-0**, Fig. 3**A**), a composition for which maximum selectivity to ethylene at low conversions is achieved.

Table 3
Catalytic results during the ethane ODH over Te-free and Te-containing catalysts.[a].

Catalyst	W/F[b]	Conversion	Selectivity (%)			Reaction rate	STY_{C2H4}[c]
	(g_{cat} h mol_{C2}^{-1})	(%)	C_2H_4	CO	CO_2	per area[d]	
F-0	16	33.7	87.4	4.0	8.6	23.0	644
F-0.01	16	52.5	77.1	5.3	17.6	21.0	1058
F-0.05	16	58.8	80.2	5.2	14.6	32.8	1225
F-0.10	16	26.4	84.5	3.6	11.9	10.7	381
F-0.17	16	5.7	88.0	3.0	9.0	5.1	85.7
S-0	65	1.9	80.9	5.9	13.2	1.21	6.57
S-0.01	65	5.4	84.5	4.5	11.0	1.38	19.5
S-0.05	65	9.3	83.0	3.5	13.4	3.30	33.0
S-0.10	65	11.2	91.4	2.1	6.4	4.47	50.8
S-0.17	65	19.3	93.4	1.7	4.9	13.7	96.2

[a] Reaction conditions: T = 390°C, C_2H_6/O_2/He molar ratio = 5/5/90.
[b] Contact time, W/F, in g_{cat} h $(mol_{C2H6})^{-1}$.
[c] Rate formation of ethylene per unit mass of catalyst, STY_{C2H4} (space time yield), in g_{C2H4} kg_{cat}^{-1} h^{-1}. Determined at ethane conversions lower than 10%.
[d] Reaction rate normalized per surface area (determined by N_2-adsorption) in 10^{-3} g_{C2H4} m^{-2} h^{-1}. Determined at ethane conversions lower than 10%.

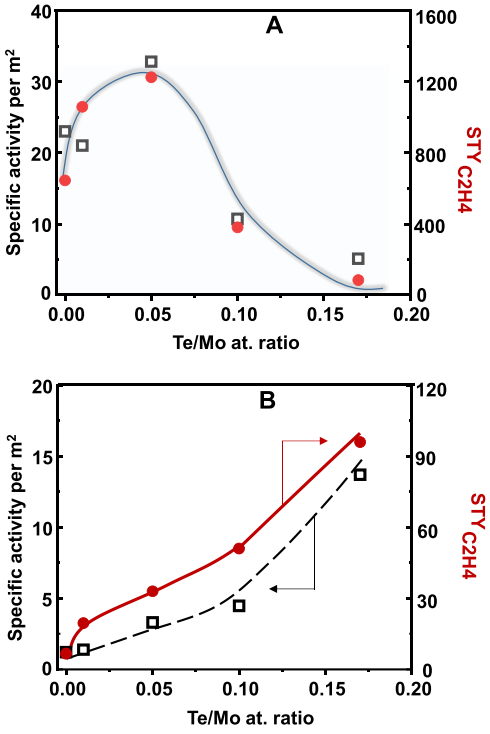

Fig. 7. Influence of the Te-content on the specific activity (activity normalized per surface area) and on the rate of product formation (STY_{C2H4}) during the ethane ODH over undoped and Te-doped MoV-Oxide catalysts heat-treated at 400°C (A) or 600°C (B). Units and experimental conditions as in Table 3.

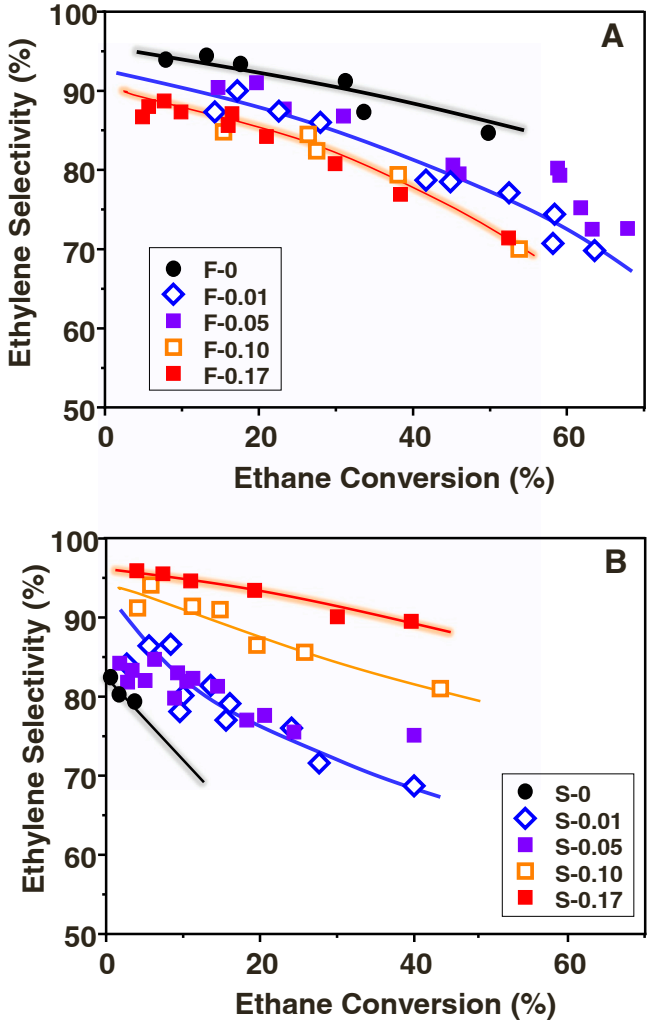

Fig. 8. Variation of the selectivity to ethylene with ethane conversion during the ethane ODH over undoped and Te-doped MoV-oxides catalysts heat-treated at 400°C (A) or 600°C (B). Experimental conditions in text.

However, for catalysts activated at 600°C, the concentration of V^{4+} reaches a maximum for catalyst with all of tellurium atoms occupying the hexagonal channels (sample **S-0.17**, Fig. 3B), as observed also for M1-containing MoVTeNbO catalysts [44], as a consequence of the interaction of V-atoms during the heat-treatment.

Fig. 9B presents the variation of the selectivity to ethylene (at 390°C and isoconversion conditions, i.e ethane conversion of 40%) with the V^{4+}/V_{total} on the surface of catalysts (determined by XPS, see Table 2). According to these results, it can be concluded that the most selective catalysts are those with the highest concentration of surface V^{4+} species.

Then, in the present article, the incorporation of Te^{4+} cations into the M1 structure produces a progressive modification in the crystal growth mode which runs in parallel with a better crystallinity (Fig. 2). In addition, it leads to the blockage of V^{4+} species onto the catalysts' surface when the samples are heat-treated at 400°C, resulting in a decrease in the selectivity to ethylene directly related to the amount of tellurium in the catalyst. The positive role of V^{4+} surface species is in agreement with previous results [64,70,71]. Thus, Millet proposed that the activation of the alkanes occurred on the vanadium sites located in M7 position of the M1 structure. Moreover, the catalytic activity of this

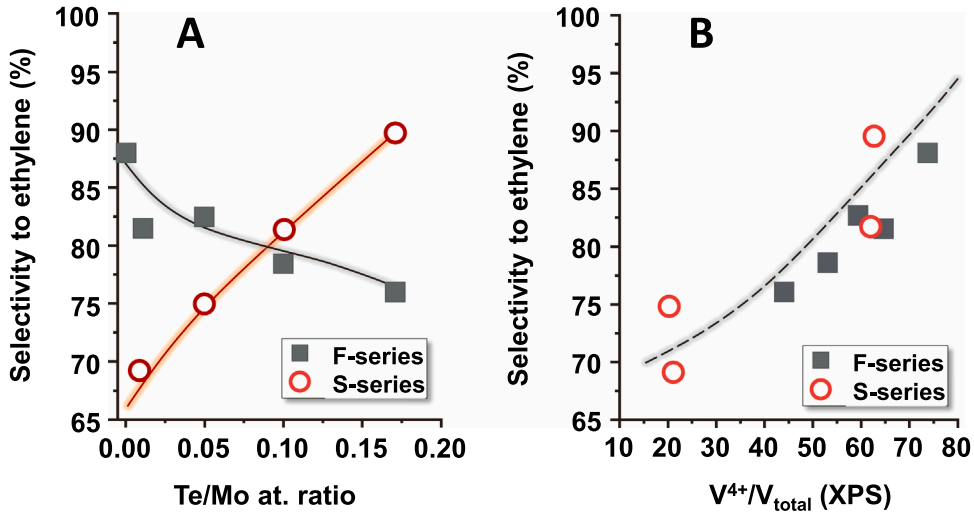

Fig. 9. Variation of the selectivity to ethylene with the Te/Mo ratio in the synthesis gel (A) or amount of V^{4+} on the catalyst surface, i.e. V^{4+}/V_{total}, determined by XPS (B) during the ethane ODH over undoped and Te-doped MoV-oxides catalysts heat-treated at 400°C (■) or 600°C ○(○). Notes: Selectivity to ethylene at 40% conversion and 390°C. Remaining experimental conditions in text.

site can be explained by the resonance form: $V^{5+}= O^{2-} \rightarrow V^{4+}\text{-}O^{-}$ [70]. However, an excess of V^{5+} in the M1 phase could favor combustion reactions [64,70,71].

Finally, the initial presence of Te^{4+} slightly modify the catalytic performance of these catalysts. This is in agreement with recent results, in which {Te-Ox} chains present in the hexagonal channels of M1 structure participate in the redox process of the catalyst [38,72–74].

Accordingly, Te-free and Te-doped catalysts present high selectivity to ethylene, but their catalytic performance strongly depends on heat-treatment temperature. Thus, for the catalysts heat-treated at 400°C, low contents of tellurium (samples **F-0.01** and **F-0.05**) favor a relatively high selectivity to ethylene, where the lowest selectivity to ethylene can be found for samples with higher Te-content (i.e. Te/Mo content in catalysts of $0.05 < x < 0.10$ as in **F-0.10** and **F-0.17**). However, Te-doped samples with Te/Mo ratios of ca. 0.05 present the highest rate of ethylene formation, STY_{C2H4} (Fig. 7 and Fig. S11), as a result of its high catalytic activity (higher than those samples with less Te) maintaining a high selectivity to ethylene.

The lower selectivity to ethylene of the catalysts with higher Te-loading, **F-0.10** and **F-0.17**, can be attributed to the large presence of V^{5+} surface species, the low micropore area/external area ratio and also to the formation of non-M1 phases such as MoO_3 (as observed by FTIR and Raman).

In an opposite trend, the higher selectivity to ethylene of the catalysts synthesized with the highest Te-loading and activated at 600°C, i.e. **S-0.10** and **S-0.17**, may be due to the preponderance of V^{4+} surface species without the presence of additional non-desired crystalline phases (as observed by FTIR and Raman) [75]. However, the low selectivity to ethylene achieved by the Te-free catalyst (**S-0**) must be unequivocally related to the scarce presence of the M1 phase.

4. Conclusions

Te-doped MoV-Oxide M1 catalysts, with $0.01 \leq$ Te/Mo at. ratio ≤ 0.17, have been prepared hydrothermally and heat-treated at 400 or 600°C in N_2, by using an optimized preparation procedure. They have been compared to undoped MoV-Oxide M1 catalyst. Characterization by XRD, IR and HRTEM confirm the presence of the M1 phase in all catalysts, regardless of the composition and the activation conditions. The presence of this phase is majority in all cases except in the case of the Te-free MoV catalyst heat treated at 600°C which is minority. Thus, the presence of Te (even at very low Te contents), strongly increase the thermal stability of the M1 phase.

The surface area and the microporosity of these materials decrease with the heat- treatment temperature. Thus, the catalysts heat-treated at 400°C show high microporosity depending on the tellurium content. On the other hand, catalysts heat treated at 600°C present lower porosity. Therefore, the addition of tellurium leads to an initial increase in the microporosity, achieving the maximum for Te/Mo ratios in the synthesis gel of 0.01 and 0.05. However, further increase in the tellurium content favours a decrease in the microporosity of these materials.

All the catalysts, Te-free and Te-containing MoV oxides, and heat-treated at 400°C, present the M1 phase as the majority crystalline phase. However, the presence of the M1 phase in the Te-free MoV catalyst heat treated at 600°C is scarce. Interestingly, the incorporation of Te atoms strongly increases the thermal stability of the M1 phase and the presence of the M1 phase becomes preponderant. Surprisingly, this effect takes place at very low Te-loadings (even at Te/Mo at. ratio of 0.01).

The observed results for ethane ODH of these catalysts suggest that their catalytic performance strongly depends on the composition and the heat-treatment temperature. For catalysts heat-treated at 400°C, the highest catalytic activity is observed for samples prepared with the lowest Te/Mo ratio in the synthesis gel, whereas for catalysts heat-treated at 600°C the catalytic activity increases when increasing the Te-content (probably as a consequence of the higher thermal stability of Te-containing catalysts).

Changes in the selectivity to ethylene have been also observed for these catalysts. Thus, for catalysts heat-treated at 400°C, the selectivity to ethylene decreases in the following order (in parenthesis the Te/Mo ratio in the synthesis gel): MoV > Te(0.01)MoV = Te(0.05)MoV > Te(0.10)MoV > Te(0.17)MoV. However, for catalysts heat-treated at 600ºC, the selectivity to ethylene decreases in the opposite trend: Te(0.17)MoV > Te(0.10)MoV > Te(0.05)MoV = Te(0.01)MoV > MoV (non-M1 structure). Overall, the most selective catalyst, especially at high ethane conversions, is that prepared with a Te/Mo in the synthesis gel of 0.17 and heat-treated at 600°C.

This divergent trend observed with the Te-loading depending on the heat treatment temperature has been explained on the basis of the different concentration of surface V^{4+} species. Then, a good correlation between the selectivity to ethylene at high ethane conversion and the concentration of V^{4+} species on the catalysts' surface is observed when considering all the studied catalysts.

Then, the presence of Te^{4+} in the M1 phase seems to stabilize the formation of V^{4+} surface species for catalysts heat-treated at 600°C, as observed also for the best MoVTeNbO catalysts [44], then favouring

high selectivity to ethylene, preventing at the same time its deep oxidation into CO_x.

CRediT authorship contribution statement

A. de Arriba: Investigation, Formal analysis, Writing – review & editing. **B. Solsona:** Conceptualization, Supervision, Writing – review & editing. **E. García-González:** Methodology, Investigation, Formal analysis, Writing. **P. Concepción:** Methodology, Investigation, Formal analysis, Writing. **J.M. López Nieto:** Conceptualization, Supervision, Project Administration, Writing – review & editing.

Declaration of Competing Interest

The authors declare that they have no known competing financial interests or personal relationships that could have appeared to influence the work reported in this paper.

Acknowledgements

The authors would like to thank the Spanish Ministry of Economy and Competitiveness for funding the projects (MINECO/FEDER): CRTl2018-099668-B-C21, PID2019-106662RBC44, MAT2017-84118-C2-1-R and SEV-2016-0683. A.A. acknowledges Severo Ochoa Excellence Program for his fellowship (BES-2017-080329). Authors would also like to acknowledge the "A-Team" of the ITQ (Dr. Miguel Palomino, Dr. Susana Valencia and Prof. Fernando Rey) for their assistance in the performance of the adsorption experiments.

Appendix A. Supporting information

Supplementary data associated with this article can be found in the online version at doi:10.1016/j.apcata.2022.118780.

References

[1] BP Energy Outlook 2020, available from: ⟨https://www.bp.com/content/dam/bp/business-sites/en/global/corporate/pdfs/energy-economics/energy-outlook/bp-energy-outlook-2020.pdf⟩ (2020).
[2] (a) T. Ren, M. Patel, K. Blok, Olefins from conventional and heavy feedstocks: energy use in steam cracking and alternative processes, Energy 31 (2006) 425–451; (b) B. Subramaniam, R.K. Helling, Cl.J. Bode, Quantitative sustainability analysis: a powerful tool to develop resource-efficient catalytic technologies, ACS Sustain. Chem. Eng. 4 (2016) 5859–5865.
[3] A. Corma, E. Corresa, Y. Mathieu, L. Savanaud, S. Al-Bogami, M.S. Al-Ghrami, A. Bourane, Crude oil to chemicals: light olefins from crude oil, Catal. Sci. Technol. 7 (2017) 12–46.
[4] F. Cavani, A. Chieregato, J.M. López Nieto, J.M.M. Millet, in: A.J.L. Pombeiro, M.F. C. Guedes da Silva (Eds.), Gas-Phase Oxidation of Alkanes, in *Alkane Functionalization*, JohnWiley & Sons, 2019, pp. 159–188.
[5] (a) Y. Gao, L. Neal, D. Ding, W. Wu, Ch Baroi, A.M. Gaffney, F. Li, Recent advances in intensified ethylene production—a review, ACS Catal. 9 (2019) 8592–8621; (b) A.M. Gaffney, J.W. Sims, V.J. Martin, N.V. Duprez, K.J. Louthan, K.L. Roberts, Evaluation and analysis of ethylene production using oxidative dehydrogenation, Catal. Today 369 (2021) 203–209.
[6] S. Najari, S. Saeidi, P. Concepción, D.D. Dionysiou, S.K. Bhargava, A.F. Lee, K. Wilson, Oxidative dehydrogenation of ethane: catalytic and mechanistic aspects and future trends, Chem. Soc. Rev. 50 (2021) 4564–4604.
[7] J.T. Grant, J.M. Venegas, W.P. McDermott, I. Hermans, Aerobic oxidations of light alkanes over solid metal oxide catalysts, Chem. Rev. 118 (2018) 2769–2815.
[8] C.A. Gärtner, A.C. van Veen, J.A. Lercher, Oxidative dehydrogenation of ethane: common principles and mechanistic aspects, ChemCatChem 5 (2013) 3196–3217.
[9] J.M. López Nieto, The selective oxidative activation of light alkanes. From supported vanadia to multicomponent bulk V-containing catalysts, Top. Catal. 41 (2006) 3–15.
[10] F. Cavani, N. Ballarini, A. Cericola, Oxidative dehydrogenation of ethane and propane: how far from commercial implementation? Catal. Today 127 (2007) 113–131.
[11] J.M. López Nieto, P. Botella, M.I. Vázquez, A. Dejoz, The selective oxidative dehydrogenation of ethane over hydrothermally synthesised MoVTeNb catalysts, Chem. Commun. 17 (2002) 1906–1907.
[12] J.M. López Nieto, P. Botella, P. Concepción, A. Dejoz, M.I. Vázquez, Oxidative dehydrogenation of ethane on Te-containing MoVNbO catalysts, Catal. Today 91–92 (2004) 241–245.
[13] Z. Han, X. Yi, Q. Xie, R. Li, H. Lin, Y. He, L. Chen, W. Weng, H. Wan, Oxidative dehydrogenation of ethane over MoVTeNbO catalyst prepared by a slurry method, Chin. J. Catal. 26 (2005) 441–442.
[14] J.S. Valente, R. Quintana- Solorzano, R. Armendariz-Herrera, G. Barragán-Rodriguez, J.M. López Nieto, Kinetic study of oxidative dehydrogenation of ethane over MoVTeNb mixed-oxide catalyst, Ind. Eng. Chem. Res. 53 (2014) 1775–1786.
[15] T.T. Nguyen, B. Deniau, P. Delichere, J.M.M. Millet, Influence of the content and distribution of vanadium in the M1 phase of the MoVTe(Sb)NbO catalysts on their catalytic properties in light alkanes oxidation, Top. Catal. 57 (2014) 1152–1162.
[16] P. Kube, B. Frank, S. Wrabetz, J. Kröhnert, M. Hävecker, J. Velasco-Vélez, J. Noack, R. Schölgl, A. Trunschke, Functional analysis of catalysts for lower alkane oxidation, ChemCatChem 9 (2017) 573–585.
[17] Y. Zhu, P.V. Sushko, D. Melzer, E. Jensen, L. Kovarik, C. Ophus, M. Sanchez-Sanchez, J.A. Lercher, N.D. Browning, Formation of oxygen radical sites on MoVNbTeOx by cooperative electron redistribution, J. Am. Chem. Soc. 139 (2017) 12342.
[18] D. Melzer, G. Mestl, K. Wanninger, Y. Zhu, N.D. Browning, M. Sánchez-Sánchez, J. A. Lercher, Design and synthesis of highly active MoVTeNb-oxides for ethane oxidative dehydrogenation, Nat. Commun. 10 (2019) 4012.
[19] A.M. Gaffney, Q. An, W.A. Goddard III, W. Diao, M.V. Glazoff, Toward concurrent engineering of the M1-based catalytic systems for oxidative dehydrogenation (ODH) of alkanes, Top. Catal. 63 (2020) 1667–1681.
[20] L. Annamalai, Y. Liu, S. Ezenwa, Y. Dang, S.L. Suib, P. Deshlahra, Influence of tight confinement on selective oxidative dehydrogenation of ethane on MoVTeNb mixed oxides, ACS Catal. 8 (2018) 7051–7067.
[21] T. Konya, T. Katou, T. Murayama, S. Ishikawa, M. Sadakane, D. Buttrey, W. Ueda, An orthorhombic Mo_3VO_x catalyst most active for oxidative dehydrogenation of ethane among related complex metal oxides, Catal. Sci. Technol. 3 (2013) 380–387.
[22] S. Ishikawa, D. Kobayashi, T. Konya, S. Ohmura, T. Murayama, N. Yasuda, M. Sadakame, W. Ueda, Redox treatment of orthorhombic $Mo_{29}V_{11}O_{112}$ and relationships between crystal structure, microporosity and catalytic performance for selective oxidation of ethane, J. Phys. Chem. C. 119 (2015) 7195–7206.
[23] S. Ishikawa, X. Yi, T. Murayama, W. Ueda, Heptagonal channel micropore of orthorhombic Mo_3VO_x as catalysis field for the selective oxidation of ethane, Appl. Catal. A-Gen. 474 (2014) 10–17.
[24] Sadakane, K. Kodato, N. Yasuda, S. Ishikawa, W. Ueda, Thermal behavior, crystal structure, and solid-state transformation of orthorhombic Mo–V oxide under nitrogen flow or in air, ACS Omega 4 (2019) 13165–13171.
[25] E.V. Lazareva, V.M. Bondareva, D.A. Svintsitskiy, A.V. Ishchenko, A.S. Marchuk, E. P. Kovalev, T.Yu Kardash, Oxidative dehydrogenation of ethane over M1 MoVNbTeO catalysts modified by the addition of Nd, Mn, Ga or Ge, Catal. Today 361 (2021) 50–56.
[26] G.A. Zenkovets, A.A. Shutilov, V.M. Bondareva, V.I. Sobolev, A.S. Marchuk, S. V. Tsybulya, I.P. Prosvirin, A.V. Ishchenko, V.Yu Gavrilov, New multicomponent MoVSbNbCeOx/SiO2 catalyst with enhanced catalytic activity for oxidative dehydrogenation of ethane to ethylene, ChemCatChem 12 (2020) 4149–4159.
[27] D.A. Svintsitskiy, T.Y. Kardash, E.V. Lazareva, A.A. Saraev, E.A. Derevyannikova, M. Vorokhta, B. Smídc, V.M. Bondareva, NAP-XPS and in situ XRD study of the stability of Bi-modified MoVNbTeO catalysts for oxidative dehydrogenation of ethane, Appl. Catal. A, Gen. 579 (2019) 141–150.
[28] T.Y. Kardash, E.V. Lazareva, D.A. Svintsitskiy, A.V. Ishchenko, V.M. Bondareva, R. B. Neder, The evolution of the M1 local structure during preparation of VMoNbTeO catalysts for ethane oxidative dehydrogenation to ethylene, RSC Adv. 8 (2018) 35903–35916.
[29] X. Tu, M. Niwa, A. Arano, Y. Kimata, E. Okazaki, S. Nomura, Controlled silylation of MoVTeNb mixed oxide catalyst for the selective oxidation of propane to acrylic acid, Appl. Catal. A- Gen. 549 (2018) 152–160.
[30] B. Chu, L. Truter, T.A. Nijhuis, Y. Cheng, Performance of phase-pure M1 MoVNbTeOx catalysts by hydrothermal synthesis with different post-treatments for the oxidative dehydrogenation of ethane, Appl. Catal. A Gen. 498 (2015) 99–106.
[31] H. Tsuji, Y. Koyasu, Synthesis of MoVNbTe(Sb)Ox composite oxide catalysts via reduction of polyoxometalates in an aqueous medium, J. Am. Chem. Soc. 124 (2002) 5608–5609.
[32] J.M.M. Millet, H. Roussel, A. Pigamo, J.L. Dubois, J.C. Jumas, Characterization of tellurium in MoVTeNbO catalysts for propane oxidation or ammoxidation, Appl. Catal. A- Gen. 232 (2002) 77–92.
[33] P. Botella, J.M. López Nieto, B. Solsona, A. Mifsud, F. Márquez, The preparation, characterization, and catalytic behavior of MoVTeNbO catalysts prepared by hydrothermal synthesis, J. Catal. 209 (2002) 445–455.
[34] D. Vitry, Y. Morikawa, J.L. Dubois, W. Ueda, Mo-V-Te-(Nb)-O mixed metal oxides prepared by hydrothermal synthesis for catalytic selective oxidations of propane and propene to acrylic acid, Appl. Catal. A-Gen. 251 (2003) 411–424.
[35] P. DeSanto, D.J. Buttrey, R.K. Grasselli, C.G. Lugmair, A.F. Volpe, B.H. Toby, T. Vogt, Structural characterization of the orthorhombic phase M1 in MoVNbTeO propane ammoxidation catalyst, Top. Catal. 23 (2003) 23–38.
[36] A. Celaya Sanfiz, T.W. Hansen, F. Girgsdies, O. Timpe, E. Rodel, T. Ressler, A. Trunschke, R. Schlögl, Preparation of phase-pure M1 MoVTeNb oxide catalysts by hydrothermal synthesis—influence of reaction parameters on structure and morphology, Top. Catal. 50 (2008) 19–32.
[37] J.M. Oliver, J.M. López Nieto, P. Botella, Selective oxidation and ammoxidation of propane on a Mo–V–Te–Nb–O mixed metal oxide catalyst: a comparative study, Catal. Today 96 (2004) 241–249.
[38] M. Aouine, T. Epicier, J.-M.M. Millet, In situ environmental STEM study of the MoVTe oxide M1 phase catalysts for ethane oxidative dehydrogenation, ACS Catal. 6 (2016) 4775–4781.

[39] W. Ueda, D. Vitry, T. Katou, Structural organization of catalytic functions in Mo-based oxides for propane selective oxidation, Catal. Today 96 (2005) 235–240.
[40] W. Ueda, D. Vitry, T. Katou, Crystalline MoVO based complex oxides as selective oxidation catalysts of propane, Catal. Today 99 (2005) 43–49.
[41] N. Watanabe, W. Ueda, Comparative study on the catalytic performance of single-phase Mo−V−O-based metal oxide catalysts in propane ammoxidation to acrylonitrile, Ind. Eng. Chem. Res. 45 (2006) 607–614.
[42] D. Vitry, Y. Morikawa, J.L. Dubois, W. Ueda, Propane selective oxidation over monophasic Mo–V–Te–O catalysts prepared by hydrothermal synthesis, Top. Catal. 23 (2003) 47–53.
[43] V.V. Guliants, R. Bhandari, J.N. Al-Saeedi, V.K. Vasudevan, R.S. Soman, O. Guerrero-Pérez, M.A. Bañares, Bulk mixed Mo–V–Te–O catalysts for propane oxidation to acrylic acid, Appl. Catal. A- Gen. 274 (2004) 123–132.
[44] P. Concepción, S. Hernández, J.M. López Nieto, On the nature of active sites in MoVTeO and MoVTeNbO catalysts: The influence of catalyst activation temperature, Appl. Catal. A.: Gen. 391 (2011) 92–101.
[45] P. Botella, P. Concepción, J.M. López Nieto, Y. Moreno, The influence of Te-precursor in Mo-V-Te-O and Mo-V-Te-Nb-O catalysts on their catalytic behaviour in the selective propane oxidation, Catal. Today 99 (2005) 51–57.
[46] W. Ueda, K. Oshihara, Selective oxidation of light alkanes over hydrothermally synthesized Mo-V-M-O (M=Al, Ga, Bi, Sb, and Te) oxide catalysts, Appl. Catal. A-Gen. 200 (2000) 135–143.
[47] W. Ueda, K. Oshihara, D. Vitry, T. Hisano, Y. Kayashima, Hydrothermal synthesis of Mo-based oxide catalysts and selective oxidation of alkanes, Catal. Surv. Jpn 6 (2002) 33–43.
[48] P. Botella, A. Dejoz, M.C. Abelló, M.I. Vázquez, L. Arrúa, J.M. López Nieto, Selective oxidation of ethane: developing an orthorhombic phase in Mo–V–X (X= Nb, Sb, Te) mixed oxides, Catal. Today 142 (2009) 272–277.
[49] P. Botella, E. García-González, J.M. López Nieto, J.M. González-Calbet, MoVTeNbO multifunctional catalysts: correlation between constituent crystalline phases and catalytic performance, Solid State Sci. 7 (2005) 507–519.
[50] J.S. Valente, H. Armendáriz-Herrera, R. Quintana-Solórzano, P. Del Ángel, A. Massó, J.M. López Nieto, Chemical, structural, and morphological changes of a MoVTeNb catalyst during oxidative dehydrogenation of ethane, ACS Catal. 4 (2014) 1292–1301.
[51] M. Baca, A. Pigamo, J.L. Dubois, J.M.M. Millet, Propane oxidation on MoVTeNbO mixed oxide catalysts: study of the phase composition of active and selective catalysts, Top. Catal. 23 (2003) 39–46.
[52] J.M. López Nieto, P. Botella, B. Solsona, J.M. Oliver, The selective oxidation of propane on Mo-V-Te-Nb-O catalysts: The influence of Te-precursor, Catal. Today 81 (2003) 87–94.
[53] I.E. Wachs, J.-M. Jehng, W. Ueda, Determination of the chemical nature of active surface sites present on bulk mixed metal oxide, Catal., J. Phys. Chem. B 109 (2005) 2275–2284.
[54] G. Mestl, In situ Raman spectroscopy for the characterization of MoVW mixed oxide catalysts, J. Raman Spectrosc. 33 (2002) 333–347.
[55] B. Solsona, M.I. Vázquez, F. Ivars, A. Dejoz, P. Concepción, J.M. López Nieto, Selective oxidation of propane and ethane on diluted Mo–V–Nb–Te mixed-oxide catalysts, J. Catal. 252 (2007) 271–280.
[56] J.C.J. Bart, F. Cariati, A. Sgamellotti, Mixed-valence effects in tellurium-molybdenum oxides, Inorg. Chim. Acta 36 (1979) 105–112.
[57] F. Ivars, B. Solsona, E. Rodríguez-Castellón, J.M. López Nieto, Selective propane oxidation over MoVSbO catalysts. On the preparation, characterization and catalytic behavior of M1 phase, J. Catal. 262 (2009) 35–43.
[58] M. Thommes, K. Kaneko, A.V. Neimark, J.P. Olivier, F. Rodríguez-Reinoso, J. Rouquerol, K.S.W. Sing, Physisorption of gases, with special reference to the evaluation of surface area and pore size distribution, Pure Appl. Chem. 87 (2015) 1051–1069.
[59] L. Annamalai, S. Ezenwa, Y. Dang, H. Tan, S.L. Suib, P. Deshlahra, Comparison of structural and catalytic properties of monometallic Mo and V oxides and M1 phase mixed oxides for oxidative dehydrogenation, Catal. Today 368 (2021) 28–45.
[60] K.Ch Kim, T.-U. Yoon, Y.-S. Bae, Applicability of using CO_2 adsorption isotherms to determine BET surface areas of microporous materials, Microp. Mesop. Mater 223 (2016) 294–301.
[61] D. Melzer, G. Mestl, K. Wanninger, A. Jentys, M. Sanchez-Sanchez, J.A. Lercher, On the promoting effects of Te and Nb in the activity and selectivity of M1 MoV-oxides for ethane oxidative dehydrogenation, Top. Catal. 63 (2020) 1754–1764.
[62] E. Pérez-Botella, R. Martínez-Franco, N. González-Camuñas, A. Cantín, M. Palomino, M. Moliner, S. Valencia, F. Rey, Unusually low heat of adsorption of CO_2 on AlPO and SAPO molecular sieves, Front. Chem. 8 (2020), 588712.
[63] E. Pérez-Botella, M. Palomino, S. Valencia, F. Rey, Zeolites and other adsorbents, in: K. Kaneko, F. Rodríguez-Reinoso (Eds.), Nanoporous Materials for Gas Storage. Green Energy and Technology, Springer, Singapore, 2019, https://doi.org/10.1007/978-981-13-3504-4_7.
[64] B. Chu, H. An, X. Chen, Y. Cheng, Phase-pure M1 MoVNbTeOx catalysts with tunable particle size for oxidative dehydrogenation of ethane, Appl. Catal. A- Gen. 524 (2016) 56–65.
[65] E.I. Ishchenko, R.V. Gulyaev, T. Yu. Kardash, E. Yu. Kardash, A.V. Ishchenko, E. Yu. Gerasimov, V.I. Sobolev, V.M. Dondareva, Effect of Bi on catalytic performance and stability of MoVTeNbO catalysts in oxidative dehydrogenation of ethane, Appl. Catal. A- Gen. 534 (2017) 58–69.
[66] A.M. Wernbacher, P. Kube, M. Hävecker, R. Schlögl, A. Trunschke, Electronic and dielectric properties of MoV-Oxide (M1 Phase) under alkane oxidation conditions, J. Phys. Chem. C. 123 (2019) 13269–13282.
[67] M. Baca, A. Pigamo, J.L. Dubois, J.M.M. Millet, Fourier transform infrared spectroscopic study of surface acidity by pyridine adsorption on the M1 active phase of the MoVTe(Sb)NbO catalysts used in propane oxidation, Catal. Commun. 6 (2005) 215–220.
[68] F. Ivars-Barceló, J.M.M. Millet, T. Blasco, P. Concepción, J.S. Valente, J.M. López Nieto, Understanding effects of activation-treatments in K-free and K-MoVSbO bronze catalysts for propane partial oxidation, Catal. Today 238 (2014) 41–48.
[69] A. Trunschke, J. Noack, S. Trojanov, F. Girgsdies, T. Lunkenbein, V. Pfeifer, M. Hävecker, P. Kube, C. Sprung, F. Rosowski, R. Schlögl, The impact of the bulk structure on surface dynamics of complex Mo–V-based oxide catalysts, ACS Catal. 7 (2017) 3061–3071.
[70] J.M.M. Millet, Mechanism of first hydrogen abstraction from light alkanes on oxide catalysts, Top. Catal. 38 (2006) 83–92.
[71] S. Benomar, A. Chieregato, A. Masso, M.D. Soriano, J.A. Vidal-Moya, T. Blasco, R. Issaadi, J.M. López Nieto, Al_2O_3-supported W–V–O bronze catalysts for oxidative dehydrogenation of ethane, Catal. Sci. Technol. 10 (2020) 8064–8075.
[72] M.-J. Cheng, W.A. Goddard III, The mechanism of alkane selective oxidation by the M1 phase of Mo–V–Nb–Te mixed metal oxides: suggestions for improved catalysts, Top. Catal. 59 (2016) 1506–1517.
[73] M.-J. Cheng, W.A. Goddard III, In silico design of highly selective Mo-V-Te-Nb-O mixed metal oxide catalysts for ammoxidation and oxidative dehydrogenation of propane and ethane, J. Am. Chem. Soc. 137 (2015) 13224–13227.
[74] J.M. Arce-Ramos, A. Genest, N. Rösch, How TeO defects in MoVTeNbO catalysts material affect the V^{4+} distribution: a computational Study, J. Phys. Chem. C 124 (2020) 18628–18638.
[75] A. de Arriba, B. Solsona, A.M. Dejoz, P. Concepción, N. Homs, P. Ramirez de la Piscina, J.M. López Nieto, Evolution of the optimal catalytic systems for the oxidative dehydrogenation of ethane: the role of adsorption in the catalytic performance, J. Catal. 408 (2022) 388–400.